AGU PUBLICATIONS

Geophysical Research Letters

Supporting Information for

The impact of basal roughness on inland Thwaites Glacier sliding.

Andrew O. Hoffman[1,2], Knut Chrisitianson[1], Nicholas Holschuh[3], Elizabeth Case[4], Jonathan Kingslake[4], Robert Arthern[5]

[1]Department of Earth and Space Sciences, University of Washington, Seattle, Washington 98195

[2]Polar Science Center, Applied Physics Laboratory, University of Washington, Seattle, Washington 98195

[3]Department of Geology, Amherst College, Amherst, Massachusetts 01002-5000

[4]Department of Earth and Environmental Sciences, Columbia University, New York, New York 10027

[5]British Antarctic Survey, Cambridge, UK

Table of Contents

S1. Overview

The supplement is organized in two sections of supplement material (figures and table) with a final text section that elaborates upon methods used in the paper. We first present all filtered topographies, surface elevation and surface velocity data used in each model experiment (Figures S1-S3). We then show inversions for all inferred friction coefficient fields (Figures S4-S5) determined from the Tikhonov regularization procedure outlined in Figure S6. Model parameters are detailed in Table S1. We also describe the power-law fitting procedure used to analytically glacier derive slip length from the topography.

S2. Data

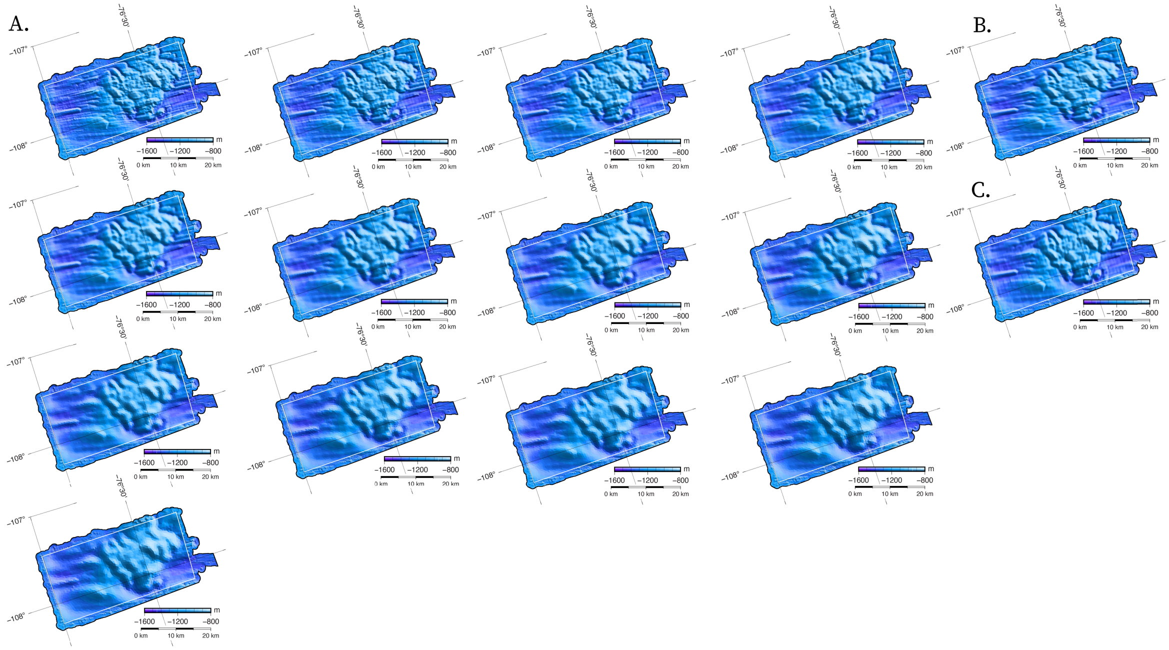

Supplementary Figure 1. The (A) topographies of the isotropically filtered grids for lower Thwaites Glacier, and the (B) along-flow and (C) transverse anisotropically filtered topographies for the lower Thwaites Glacier grid.

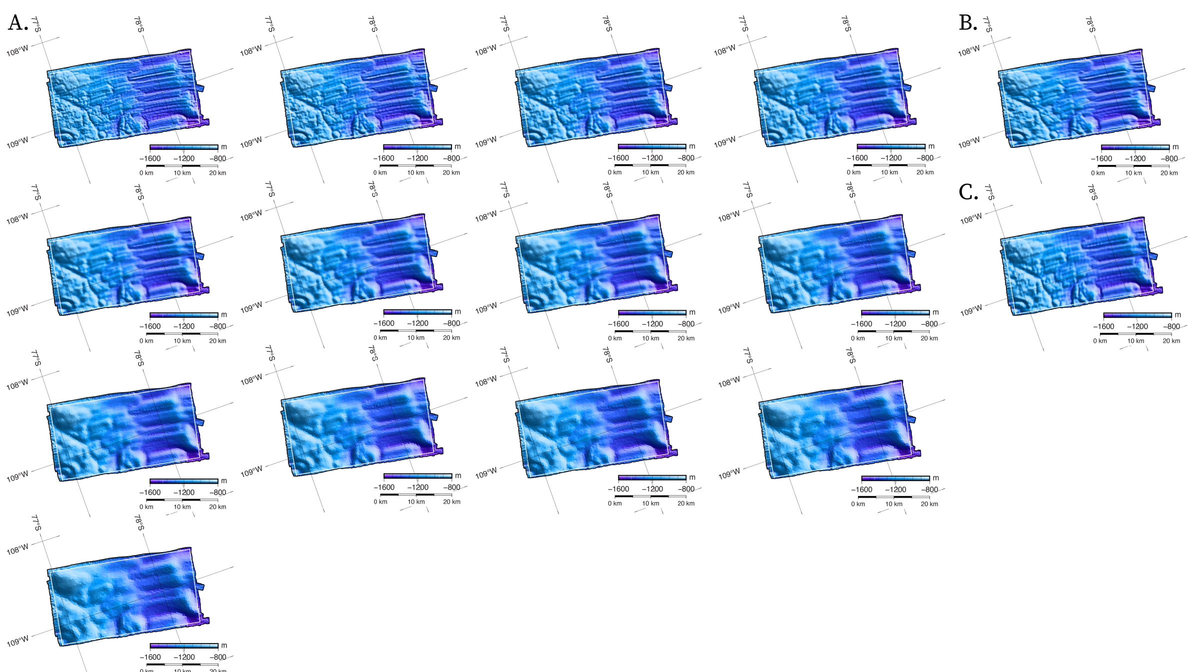

Supplementary Figure 2. The (A) topographies of the isotropically filtered grids for upper Thwaites Glacier, and the (B) along-flow and (C) transverse anisotropically filtered topographies for the upper Thwaites Glacier grid.

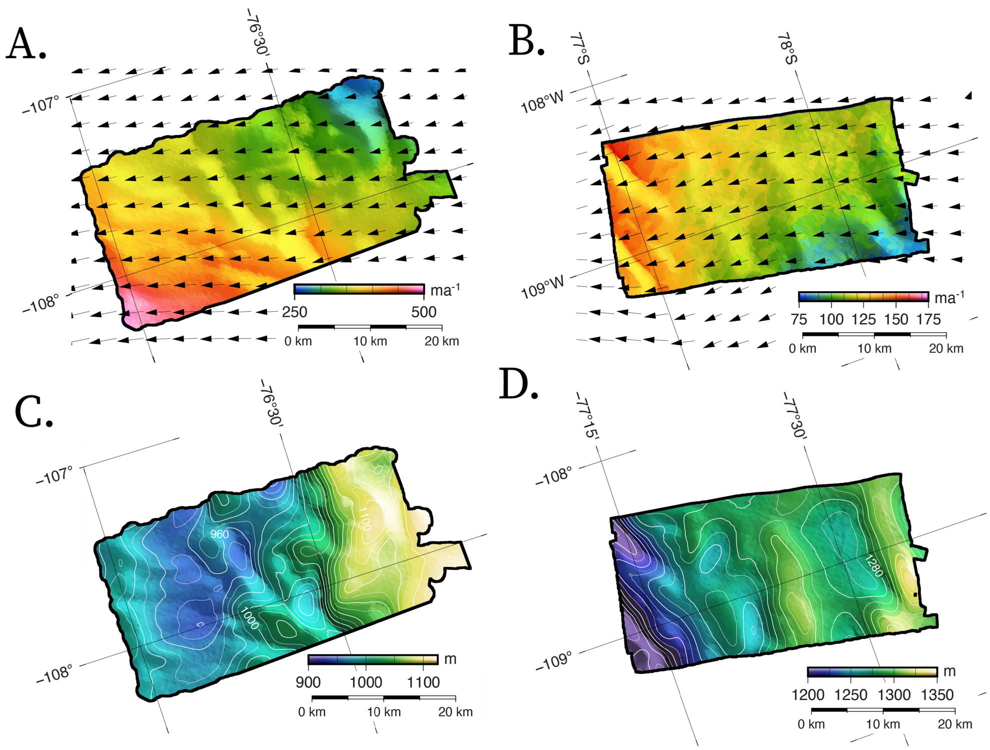

Supplementary Figure 3. The (A, B) surface velocity and (C, D) surface elevation for the lower Thwaites and upper Thwaites grids. Note, color maps are scaled uniquely for each grid.

S3. Inversions

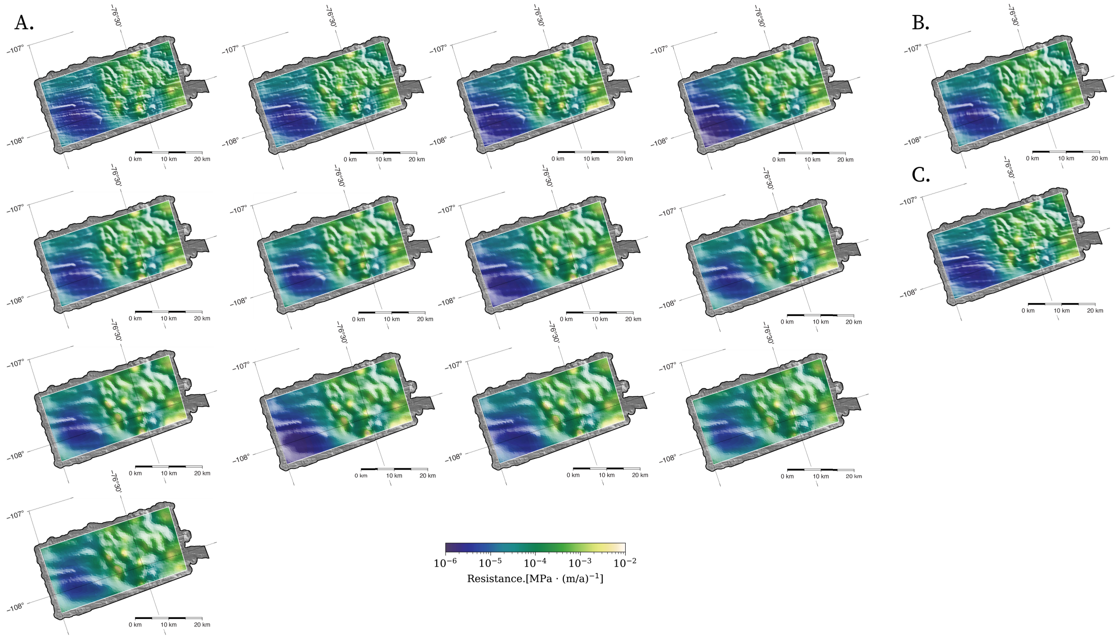

Supplementary Figure 4. The (A) inferred friction coefficient of each of the isotropically filtered lower Thwaites grid simulations, and the (B) along-flow and (C) transverse anisotropically filtered topographies for the lower Thwaites Glacier grids.

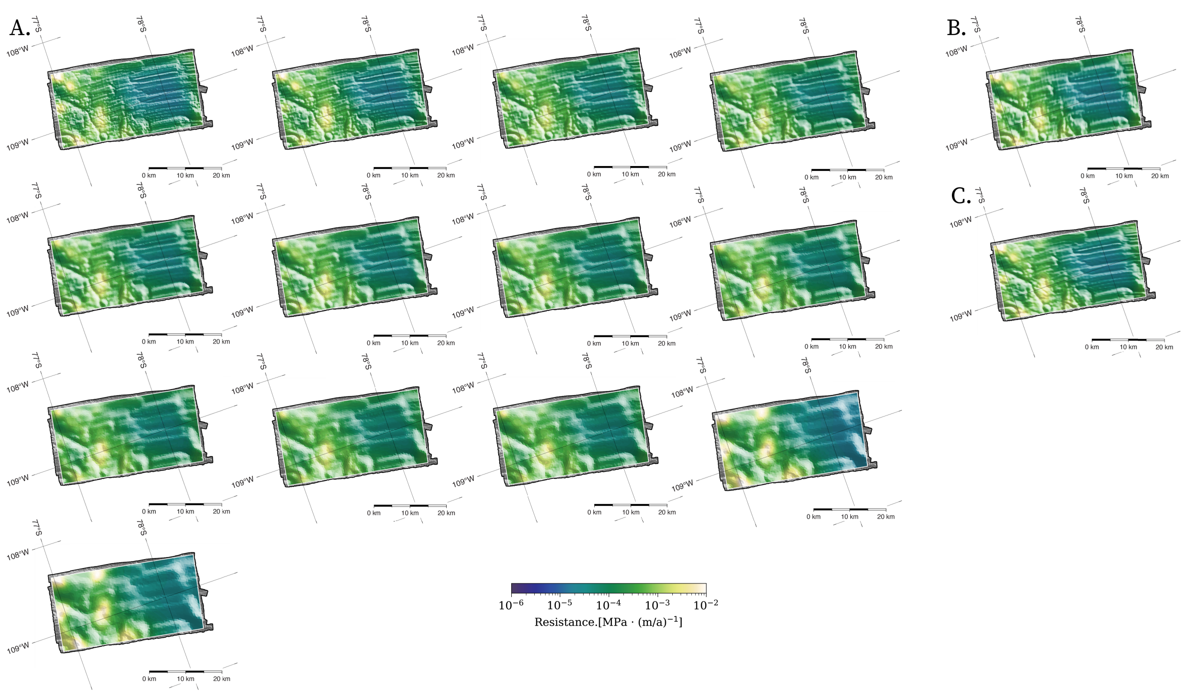

Supplementary Figure 5. The (A) inferred friction coefficient of each of the isotropically filtered upper Thwaites grid simulations, and the (B) along-flow and (C) transverse anisotropically filtered topographies for the upper Thwaites Glacier grids.

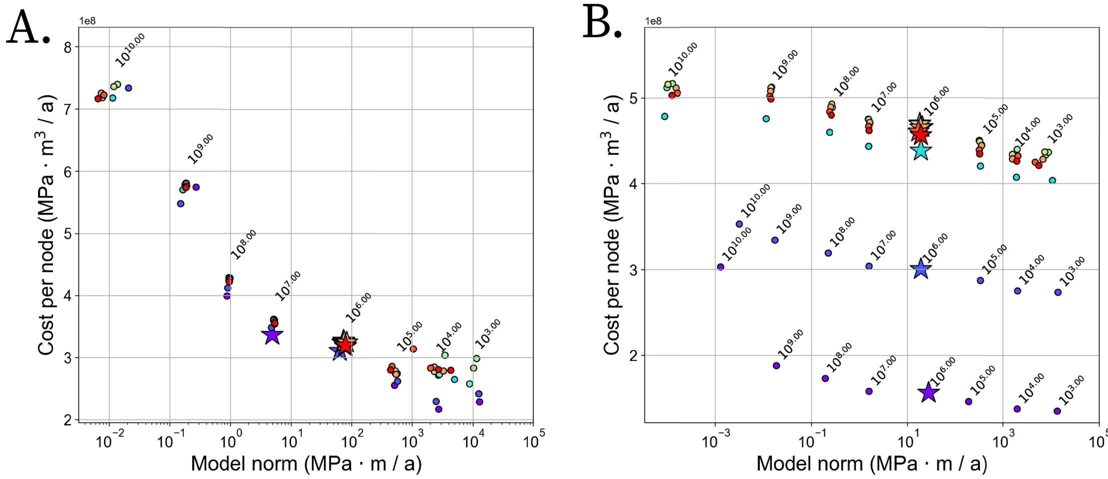

Supplementary Figure 6. The Tikhonov regularization curves (cost function plotted against the mean square gradient of beta for $\log_{10} \lambda = 10e^3, 10e^4, 10e^5, \ldots 10e^{10}$) for the (A) lower Thwaites and the (B) upper Thwaites grids where rainbow colors indicate model grid resolution (purple is highest resolution, blue second highest etc.). Between $10e^6$ and $10e^7$, the cost function increases dramatically, and the L-curve method would select a value in this range as the appropriate regularization parameter (indicated with a star). For both the lower Thwaites and upper Thwaites grids, the highest resolution model domain minimizes the most cost per node.

Parameter	Value	Units	Description
A_0	$3.985e^{-13}$	$MPa^{-3} \cdot yr^{-1}$	Spatially uniform rate factor
Q	$60e^3$	J	Spatially uniform activation energy (Patterson 2010)
R	8.314	$J/mol \cdot K$	Ideal gas constant
λ	$10e^6$	$-$	Tikhonov regularization coefficients
n	3	$-$	Glen's flow law exponent
m	1	$-$	Basal sliding relation exponent

Supplementary Table 1. Table of model parameters used across all full-Stokes simulations.

S4. Analytic Slip Length Calculation

In glacier sliding theory, slip length (L) is defined as:

$$L = \frac{\eta}{\beta} \tag{1}$$

where η is ice viscosity and β is the basal drag coefficient. If the slip length is larger than the ice thickness, the basal drag is too small to induce shear in the ice column, and ice slides over the substrate at a uniform velocity with depth (plug flow). If the slip length is smaller than the ice thickness, then basal drag can induce substantial shearing through the ice column, resulting in a depth-variable velocity profile. Slip length is thus a useful metric for distinguishing the ice-flow regime.

We compare slip lengths calculated from our modeled parameter fields to slip lengths calculated using analytic theory for form drag for ice flow over an undulating bed that requires only bed roughness power spectra as an input (Schoof, 2002). Similar to Hogan et al. (2020), we approximate one-sided periodograms of the along-flow bed roughness profiles derived from the radar swath topographies (Holschuh et al., 2020) using an inverse square power law (equivalent to a random-walk elevation profile), where the periodogram component (P_n) associated with each frequency band can be fit by:

$$P_n = A f_n^{-2} \tag{2}$$

where A is a fit coefficient with units of length and $f_n = n/a$ is the center frequency of a frequency band of width $1/a$, a is the length of the fit window, and $n = 1 \ldots N$ with N being the total number of components in the periodogram (here N=256). Following Schoof (2002) and Hogan et al. (2020), for sufficiently high wavenumbers ($k_n \gg 1/H$ where H is ice thickness) the basal drag components are given by:

$$\beta_n = 16\eta\pi^3 A a^{-1} f_n. \tag{3}$$

The total form drag coefficient can then be approximated by:

$$\beta = \sum_{n=1}^{N} \beta_n = 16\eta\pi^3 A a^{-2} \sum_{n=1}^{N} n = 8\eta\pi^3 A a^{-2} N(N+1) \tag{4}$$

and if $\lambda_n \ll a$ so $N \gg 1$, then

$$\beta = 8\eta\pi^3 A \lambda_N^{-2}. \tag{5}$$

Applying the definition of slip length then gives:

$$L = \frac{\lambda_N^2}{8\pi^3 A}. \quad (6)$$

We apply this analytic theory to our swath topographies to calculate the slip lengths associated with form drag. First, we extract bed topography at 25m posting from the radar swath topography point cloud (Holschuh et al., 2020) at each point in the point cloud along 6.4km long flowlines (distance chosen to be similar to Hogan et al. (2020)) determined using the simulation reference surface velocity field. After removing the linear trend from the bed elevation profile and applying a Hamming window, we calculate the one-sided periodogram using Welch's method (Welch, 1967). The inverse square power law coefficient A was calculated using non-linear least squares fitting. The slip length calculated following Equation 6 is plotted at the center point of each flowline.

S5. Consistency with observed subglacial lake activity?

An active subglacial lake boundary (lake Thw124; Smith et al., 2017) identified from satellite altimetry lies partially within the lower Thwaites grid. The inferred shear stress inside the lake boundary is nonzero. Satellite observations suggest variability in the lake fill-drain levels on Thwaites Glacier (Hoffman et al., 2020), so volume change estimates of lakes on Thwaites Glacier derived from satellite altimetry are difficult to relate to changes in lake geometry. Because the lake geometry is unknown for the observational period used to constrain the snap-shot inversions, we do not know how much of the lake is buoyantly supporting the overlying ice. This lake had drained prior to the epoch of the surface observations used to constrain the inversion, so the non-zero drag may be evidence of ice regrounding; however, independent GNSS observations suggest that ice velocity is insensitive to lake fill-drain cycles, which would predict low shear stress values in the vicinity of the Thwaites lakes independent of whether the lake is full or empty (Hoffman et al., 2020). The nonzero drag inside the lake could also represent resistance from topographic pinning points that may always protrude above the reported lake depth (Smith et al., 2017; Hoffman et al., 2020), which at ~20 m, is below the root mean square amplitude of subglacial roughness in the boundary of the lake and motivates further study of lake influence on ice-sheet mechanics and glacier sliding.
In the two-dimensional spectral variance of 6.0 km windowed bed topography, we see the first indication from independent subglacial datasets of spatial changes in bed properties consistent with the Thw124 lake position. Over the lake outline boundary, the bed appears to be substantially smoother than the surrounding topography (Figure 3A). The SAR focused radargrams, however, show no unambiguous evidence of an ice-lake interface. This suggests that there may not be dielectric contrast across the lake interface that is distinguishable from a wet sediment interface and/or that this interface is very rough.

S6. Simulations over a uniformly sloped bed topogaphy

Fitting a plane to the high-resolution topographies, we can simulate ice flow over a flat bed for each grid. From these simulations we can relate the basal drag to the more the more traditional horizontal shear stress (a global variable) and compare again the resistance and normal pressure fields. The patterns of the inferred resistance fields are similar to the smoothed topographies. The cost per node for each grid is substantially higher than the isotropically smoothed experiments.

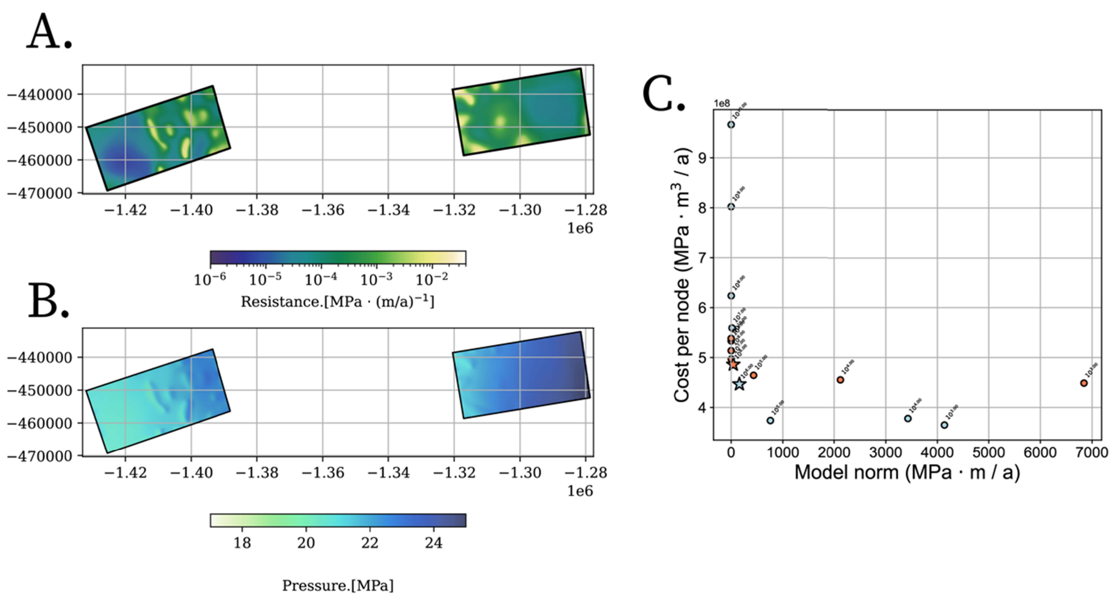

Supplementary Figure 7. (A) The basal resistance fields, (B) the normal pressure fields and the (C) Tikhonov regularization curves (cost function plotted against the mean square gradient of beta for $\log_{10}\lambda = 10e^3, 10e^4, 10e^5, \ldots 10e^{10}$) for the lower Thwaites (light blue) and the upper Thwaites (coral) flat grids. Again, near $10e^6$ the cost function increases dramatically, and the L-curve method would select a value in this range as the appropriate regularization parameter (indicated with a star). The fields in (A) and (B) are the fields associated with this choice of regularization. The cost per node for both simulations were 15% (lower thwaites) and 5% (upper thwaites) greater than the most isotropically smoothed experiments.

References

Hogan, K. A., R. D. Larter, A. G. C. Graham, R. Arthern, J. D. Kirkham, R. Totten Minzoni, T. A. Jordan, R. Clark, V. Fitzgerald, A. K. Wåhlin, J. B. Anderson, C.-D. Hillenbrand, F. O. Nitsche, L. Simkins, J. A. Smith, K. Gohl, J. E. Arndt, J. Hong, and J. Wellner, 2020. Revealing the former bed of Thwaites Glacier using sea-floor bathymetry: implications for warm-water routing and bed controls on ice flow and buttressing. The Cryosphere 14, 2883–2908, doi:10.5194/tc-14-2883-2020.

Holschuh, N., K. Christianson, J. Paden, R. B. Alley, and S. Anandakrishnan, 2020. Linking postglacial landscapes to glacier dynamics using swath radar imaging at Thwaites Glacier, Antarctica. Geology 48, 268–272, doi: 10.1130/G46772.1.

Hoffman, A., K., Christianson D., Shapero B., Smith, I., Joughin (2020), Heterogenous thinning and subglacial lake drainage on Thwaites Glacier, The Cryosphere. 14(12), 4603–4609. doi:10.5194/tc-14-4603-2020

Schoof, C., 2002. Basal perturbations under ice streams: form drag and surface expression. Journal of Glaciology 48, 407–416.

Smith, B., N., Gourmelen, A., Huth, and I., Joughin (2017), Connected subglacial lake drainage beneath Thwaites Glacier, West Antarctica. The Cryosphere. 11, 451–467. doi:10.5194/tc-11-451-2017

Welch, P. D., 1967. The Use of Fast Fourier Transform for the Estimation of Power Spectra: A Method Based on Time Averaging Over Short, Modified Periodograms. IEEE Transactions on Acoustics, Speech, and Signal Processing 15, 70–73.